Desalination and Water Treatment
www.deswater.com

doi: 10.5004/dwt.2018.23264

136 (2018) 7–19
December

Parametric study of an integrated organic Rankine/reverse Brayton refrigeration cycle and multiple-effect desalination unit

Sami M. Alelyani[a], Jonathan A. Sherbeck[a], Zhaoli Zhang[b], Weston K. Bertrand[a], Patrick E. Phelan[a,*]

[a]*School for Engineering of Matter, Transport and Energy, Arizona State University, Tempe, Arizona 85287-6106, USA, Tel. +1 (480)965 1625; Fax: +1 (480)727 9321; emails: phelan@asu.edu (P.E. Phelan), smalelya@asu.edu (S.M. Alelyani), jonathan.sherbeck@asu.edu (J.A. Sherbeck), wbertran@asu.edu (W.K. Bertrand)*
[b]*School of Mechanical Engineering, Southwest Jiaotong University, Chengdu 610031, China; email: zhangzl_sju@163.com (Z. Zhang)*

Received 25 June 2018; Accepted 9 October 2018

ABSTRACT

This study explores the opportunity of a combined cooling, desalination, and power (CCDP) unit that is thermally driven using low- to mid-grade heat input of 1,940 kW_{th} (enthalpy of vaporization of steam at 200°C and mass flow rate of 1 kg/s). The proposed CCDP system is comprised of a Rankine cycle that partially drives a gas refrigeration cycle by means of shaft work and thermally drives a multiple-effect distillation (MED) unit by harnessing the rejected heat of condenser. Based on our thermodynamic model, the proposed CCDP system is more efficient from an energy-saving viewpoint compared with stand-alone systems that deliver the same services provided if there are ≥8 MED effects (units). Furthermore, the proposed polygeneration system is able to produce nearly 188 kW_e of electrical power output, 116 kW_{th} of cooling capacity, and 25.6 m^3/h of freshwater capacity when water is employed as a working fluid and air as a refrigerant. In addition, the CCDP system attains an exergy efficiency of ≈42% and a primary energy-saving ratio of 28%. Because an organic Rankine cycle is promising for the conversion of low- and mid-grade heat to electricity, various organic working fluids are investigated. The results show that when propane is used instead of water, the freshwater capacity rises by 3.4%.

Keywords: Tri-generation; Polygeneration; Combined cooling and power; Combined cooling, heating, and power; Combined cooling; Desalination; Power

1. Introduction

A polygeneration system is an improved version of a cogeneration system in which more than two products are attained such as electricity, refrigeration, or freshwater. Combinations of different types of conventional and renewable energy sources such as fossil fuels or solar thermal energy can be leveraged together into one cycle that provides various services such as electricity, refrigeration, desalinized water, etc. Such systems are capable of ensuring high overall energy conversion efficiency with less environmental impact compared with conventional systems. Furthermore, polygeneration systems are more effective than stand-alone systems in facing energy price demand fluctuations, which is mutually beneficial to both owners and end-users.

Freshwater demand has gradually increased due to the rapid growth of population and domestic, industrial, and agricultural use. Seawater desalination has been the main, if not only, source of clean water in regions where physical water scarcity is the main challenge [1]. Moreover, drought and desertification have been increasing dramatically in regions across the world for the past few years, resulting from deficiencies in surface and groundwater [2,3]. Refrigeration and air-conditioning demands are also anticipated to increase

* Corresponding author.

from the rise of global temperatures. Consequently, the environmental impact grows increasingly worse because many common refrigerants in use today pose a threat to the environment due to their global warming potential and ozone depletion potential [4].

In a recent review, Murugan and Horak [5] discussed the research efforts and developments that have been conducted regarding poly- and trigeneration, a subset of polygeneration in which three outputs are generated. They concluded that the selection of the energy conversion device, such as gas turbines and organic Rankine cycles (ORCs), and its size are extremely important for residential and industrial applications. The location of the polygeneration plant is a significant factor to determine the most desirable products. For instance, local climate would play a role in determining the plant configuration and its possible products for an off-grid plant. Thus, they recommended thst feasibility studies should be carried out for the installation of a polygeneration system, because every system is different.

Anvari et al. [6] performed a thermoeconomical study on a combined cooling, heating, and power (CCHP) system that consists of three sections, namely, gas turbine and heat recovery steam generator (GT-HRSG), regenerative organic Rankine cycle (RORC), and absorption refrigeration cycle based on LiBr-H_2O. The result showed that adding an RORC and absorption refrigeration cycle to the GT-HRSG cycle increases the overall exergetic efficiency of the CCHP system by 2.5% and 0.75%, respectively, with a 5.5% and 0.45% increase in the total investment cost of the trigeneration cycle.

Ortega-Delgado et al. [7] performed a parametric study of a multiple-effect distillation (MED) unit with a steam ejector—widely known as multiple effect distillation with thermal vapor compression (MED-TVC)—coupled with a Rankine cycle (RC) power block. They studied the effect of the motive and suction steam pressures on the MED-TVC performance, freshwater capacity, and other key variables. They concluded that there is an optimum value of the heat transfer area of the evaporator after the suction point and optimum position of the steam ejector for every suction and motive steam pressure, respectively. When electricity demand is high, it was recommended to extract low-pressure motive steam and place the steam ejector close to the fifth effect in order to maximize the electric power production at the expense of the MED-TVC efficiency. On the other hand, extracting high-pressure motive steam from the RC turbine and locating the thermocompressor closer to the last effect is desirable when electricity demand is low to enhance the MED-TVC performance.

Mohan et al. [8] technically and economically examined the advantages of harnessing the excess waste heat from a gas turbine and rejected heat from a steam RC condenser in a combined power plant in the United Arab Emirates. The trigeneration system was optimized based on the cooling demands of the neighboring community to simultaneously produce electricity, freshwater using air gap membrane distillation, and cooling using LiBr-H_2O absorption refrigeration system. The proposed trigeneration system was projected to have an energy-conversion efficiency of about 83% compared with 51% for the combined cycle power plant with a payback period of only 1.4 years with cumulative net present value of $66 million over the project lifetime.

Akbari et al. [9] analyzed the effect of the turbine inlet pressure and evaporator outlet temperature on a combined cooling, clean water, and power system from energy and exergy perspectives. The polygeneration system consists of a Kalina cycle[1], a LiBr-H_2O heat transformer, and a water desalination system using a geothermal hot water heat source at 124°C. The energy and exergy efficiencies of the system were found to be about 17% and 65%, respectively, with a maximum freshwater production of 1.32 m^3/h. Sahoo et al. [10] studied the viability of coupling a hybrid solar-biomass power plant with cooling using an LiBr-H_2O absorption system and desalination using an MED system in a polygeneration process in India. It was found that the net equivalent power for a polygeneration system increases by 18.2% compared with a conventional power plant with stand-alone cooling and desalination systems.

Ameri and Jorjani [11] conducted exergy and economic analyses on an integrated system comprised of a Brayton cycle with a heat recovery steam generator (HRSG), an ORC, and an MED unit. The gas turbine exhaust energy is initially harnessed by the MED unit by means of employing a single-pressure HRSG before it drives the ORC. It was concluded that the optimum power and freshwater capacities are very sensitive to the MED evaporator approach temperature. Among three organic working fluids, R134a achieved the highest exergy efficiency.

Recently, Salimi and Amidpour [12] investigated the effect of the integration of different desalination systems on cogeneration system performance by utilizing the *R*-curve tool in order to identify the most effective way to decrease the operating cost. They found that the integration of thermally and electrically driven desalination units can result in either the improvement or impairment of the overall cogeneration efficiency based on the operating conditions of the cogeneration system. In particular, they demonstrated that the integration of a 17.8 MW_{th} MED unit could either provide 28.97 MW_{th} fuel savings or cause 47.84 MW_{th} excess fuel consumption.

We propose here a combined cooling, desalination, and power (CCDP) system that is comprised of Rankine power and gas refrigeration (reverse Brayton) cycles, plus a thermally driven desalination unit. This extends our previous introduction of a unit that produces shaft power and refrigeration, but not desalination [13]. The heat rejection from the condenser of the RC is exploited to drive the desalination unit that is based on MED technology. Primarily, our proposed CCDP system utilizes water and air as the working fluid and refrigerant, respectively, which are non-hazardous and environmental friendly with the aim of minimizing carbon emissions. The combined system is designed to be located by a large body of saltwater such as the ocean and to provide freshwater, refrigeration, and power on demand, which makes it potentially attractive to remote and off-grid areas.

1 The Kalina cycle is a thermodynamic process that converts thermal energy into mechanical power. It uses a mixture of two fluids as working fluid in order to extract more heat from the heat source than a conventional Rankine cycle because heat addition takes place at varying temperature even during phase change.

2. System configuration

A schematic diagram of the proposed CCDP system is shown in Fig. 1. It can be observed from Fig. 1 that the RC's turbine is connected with the compressor, the turbine of the gas refrigeration cycle, and the generator through the same shaft in order to maximize the shaft power output. Nevertheless, this might not always be the case especially if the required cooling (refrigeration) load is irregular in which the gas refrigeration sub-cycle is preferably fed by electrical power via a generator that produces electricity from the Rankine power sub-cycle.

The MED subsystem consists of multiple effects (cells) in which salt and water are separated by vaporizing some of the water content. Flow is driven from cell to cell by maintaining successively decreasing pressure levels. A cascading flow of heat is driven from cell to cell by maintaining successively decreasing temperature levels, corresponding to the decrease in vapor–liquid equilibrium temperature with increasing brine salinity. Rejected heat via the RC's condenser is proposed to provide the required heat to the first effect of the MED desalination system. Note that the mass flow rate of the seawater in the MED unit (stream F) is determined from the rejected heat of the Rankine and reverse Brayton cycles to increase the seawater temperature of 27°C to the top brine (first effect) temperature of 66°C. Incoming seawater is first introduced to the MED subsystem (stream S) by condensing the steam in a final condenser, which is produced by the last effect. Over 60% of incoming saltwater gets rejected back to the source (stream R) after exchanging heat with the MED's condenser, while the rest is pumped to the first effect (stream F). On its way to the first effect, saltwater is preheated by the gas refrigeration cycle (between points 6 and 7) and partially condenses the steam generated in each effect.

Following the stream labels in Fig. 2, the brine stream (BC_{i-1}) from the preceding effect flashes as it is introduced to the effect (i) because it is superheated at the effect's operating pressure. The remaining brine (BF_i) is then sprayed over a bundle of evaporation tubes, where steam is generated and the rest of the brine stream (BC_i) goes to the succeeding effect. The circulating steam inside the tubes (VM_{i-1}), from the preceding steam mixer, provides the heat needed for evaporation. The generated steam gets partially condensed (LP_i) by preheating incoming seawater (swP_{i+1}), while the rest of the steam (vP_i) is transported to provide the heat needed for the following effect.

3. Mathematical modeling

The mathematical model of our proposed CCDP system is based on a combined model of three separate thermodynamic models, namely, the Rankine power cycle, the gas refrigeration (reverse Brayton) cycle, and the MED desalination unit. Initially, each subsystem was modeled and validated separately before integrating them with each other to form our proposed CCDP system in Fig. 1. The following

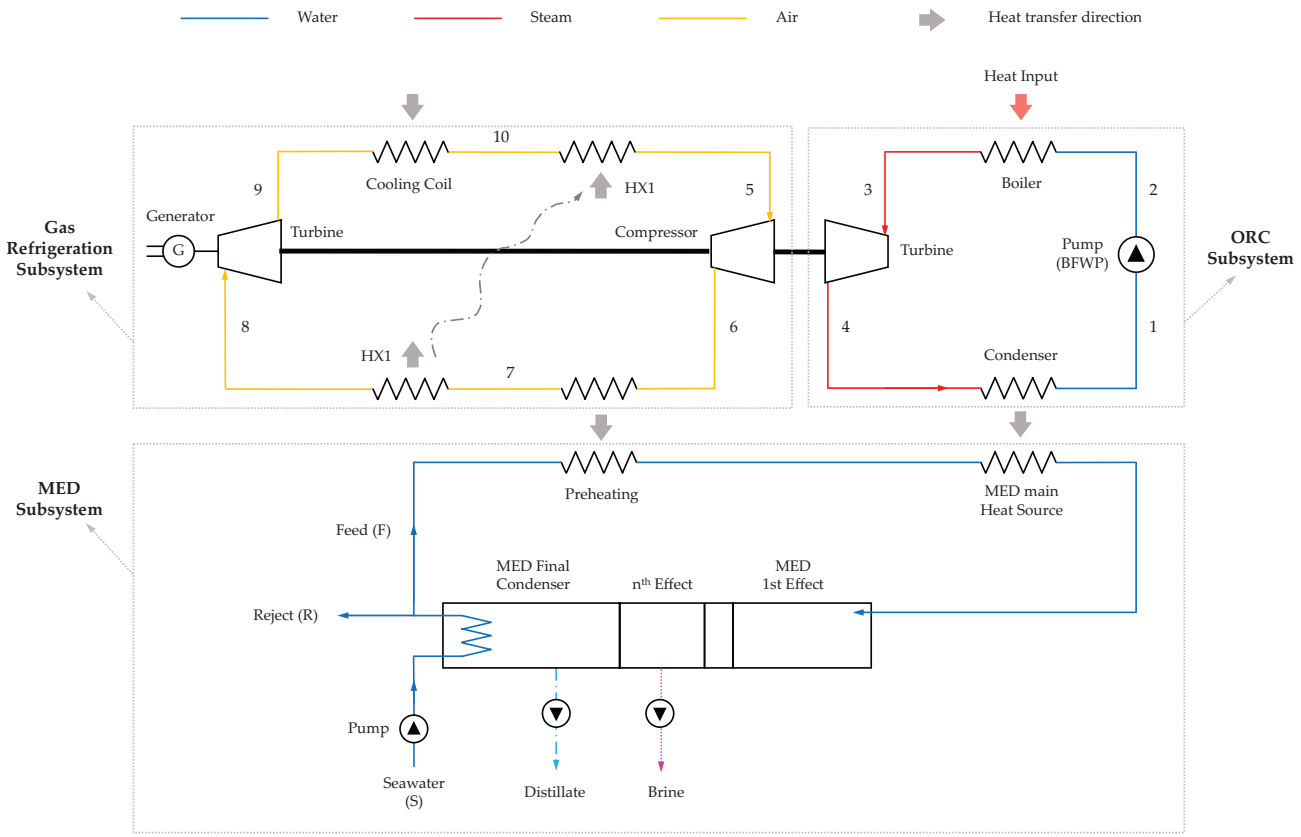

Fig. 1. Schematic diagram of the combined cooling, desalination, and power (CCDP) system.

assumptions are applied for the thermodynamic mathematical model:

- Steady-state operation with negligible kinetic and potential energy.
- Heat losses and pressure drops in the components and piping are not considered.
- The distilled freshwater is salt free.
- During phase-change processes, the bulk liquid and vapor flows are at equilibrium in each cross section.

The mass balance (continuity), energy balance (the first law of thermodynamics), and exergy balance (the second law of thermodynamics) are performed for each component of the system based on the abovementioned assumptions. The Rankine power and gas refrigeration cycles can be directly modeled using widely known models as presented by Cengel and Boles [14] and Michael and Howard [15]. For this reason, this study will only present the MED mathematical models, in addition to the main parameters to the overall system performance.

3.1. MED thermodynamic model

The MED subsystem consists primarily of multiple effects and a condenser. Mass, energy, and exergy balances are performed for a typical cell, which can be divided into six control volumes as illustrated in Fig. 2, in order to simplify the analysis as recommended by [16–18]. With reference to Fig. 2, the mass and energy balance equations of the MED unit are derived and listed in Appendix A.

3.2. System performance indicator

For polygeneration systems, Rosen and Le [19] recommended the use of exergy (second law) efficiency as a system performance indicator. Unlike energy (first law) efficiency, the exergy efficiency takes into account the quality of heat and energy and can be defined as the fraction of the useful exergy to the total exergy input:

$$\eta_{\text{exergy}} = \frac{\dot{W}_{\text{ele}} + \dot{E}_{\text{cool}} + \dot{W}_{\text{MED,min}}}{\dot{E}_{\text{hs}}} \tag{1}$$

where $\dot{W}_{\text{ele}}$ is the electrical power output and $\dot{W}_{\text{MED,min}}$ is the least amount of work required to separate salt and water as calculated in Appendix A. $\dot{E}_{\text{cool}}$ and $\dot{E}_{\text{hs}}$ (kW) are the exergy rates associated with the cooling capacity and heat source input, respectively, in which $\dot{E}$ can generally be calculated as follows:

$$\dot{E} = \dot{m} \cdot \left[\left(h_{\text{in}} - h_{\text{out}} \right) - T_o \left(s_{\text{in}} - s_{\text{out}} \right) \right] \tag{2}$$

where $\dot{m}$, h, and s are mass flow rate, specific enthalpy, and specific entropy, respectively; and T_o is the temperature at the dead state. In order to compare the proposed CCDP system with conventional stand-alone cooling, desalination, and power systems from an energy-savings perspective, the primary energy-saving ratio (PESR) can be applied. Principally, the PESR is the ratio of the amount of energy savings of the

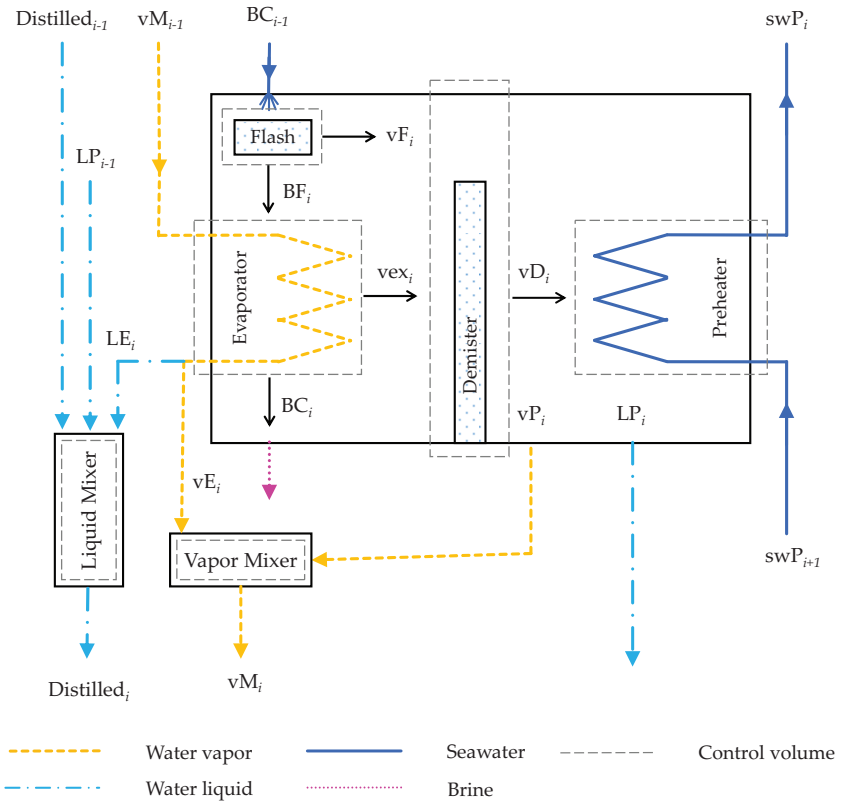

Fig. 2. Schematic diagram of a typical MED effect.

combined system compared with the energy consumption of the reference separate systems [20–22], and is expressed as follows:

$$\mathrm{PESR} = \left(\frac{F_s - F_c}{F_s}\right) \times 100\% = \left(1 - \frac{F_c}{F_s}\right) \times 100\% \tag{3}$$

where F_s and F_c are the fuel energy consumption for the separate reference and combined systems, respectively.

Fig. 3 depicts the energy flows of the proposed CCDP system, while Fig. 4 shows the reference stand-alone cooling, desalination, and power systems. Thus, the fuel energy consumptions F_s and F_c can be expressed as follows:

$$F_c = \frac{\dot{Q}_{hs}}{\eta_b} \tag{4}$$

$$F_s = F_{\mathrm{grid}} + F_b \tag{5}$$

where $\dot{Q}_{\mathrm{hs}}$ is the rate of main heat source input, ηb is the boiler efficiency, F_{grid} is the electricity consumed from the electrical grid, and F_b is the fuel consumption associated with the stand-alone MED unit, and can be calculated based on Fig. 4 as follows:

$$F_{\mathrm{grid}} = \frac{\dot{W}_{\mathrm{ele}}}{\eta_{\mathrm{grid}}} + \frac{\dot{Q}_{\mathrm{cool}}}{\mathrm{COP}_{\mathrm{ref}} \times \eta_{\mathrm{grid}}} \tag{6}$$

where η_{grid} and $\mathrm{COP}_{\mathrm{ref}}$ represent an average power plant efficiency with a constant value of 33% and cooling coefficient of performance (COP) with a value of 4.5 as in large-capacity vapor-compression chillers at standard conditions, respectively [21]:

$$F_b = \frac{\dot{Q}_{\mathrm{MED,input}}}{\eta_b} \cdot \frac{\mathrm{PR}}{\mathrm{PR}_{\mathrm{ref}}} \tag{7}$$

$$\mathrm{PR} = \frac{\dot{m}_{\mathrm{Distilled}} \cdot h_{\mathrm{fg}}}{\dot{Q}_{\mathrm{MED,\ input}}} \tag{8}$$

where PR is the performance ratio of the MED unit which is defined as the mass of desalinated water produced ($\dot{m}_{\mathrm{distilled}}$ in kg/s) per thermal energy input ($\dot{Q}_{\mathrm{MED,\ input}}$ in $\mathrm{kW_{th}}$) which is equal to the heat rejected by the RC's condenser. h_{fg} is the enthalpy of vaporization of H_2O at 73°C which corresponds to 2326 kJ/kg, and $\mathrm{PR}_{\mathrm{ref}}$ represents the performance ratio reference with a constant value of 10 [23,24]. It is worth noting that the proposed CCDP system cannot save energy when the PESR value is negative compared with the stand-alone reference systems.

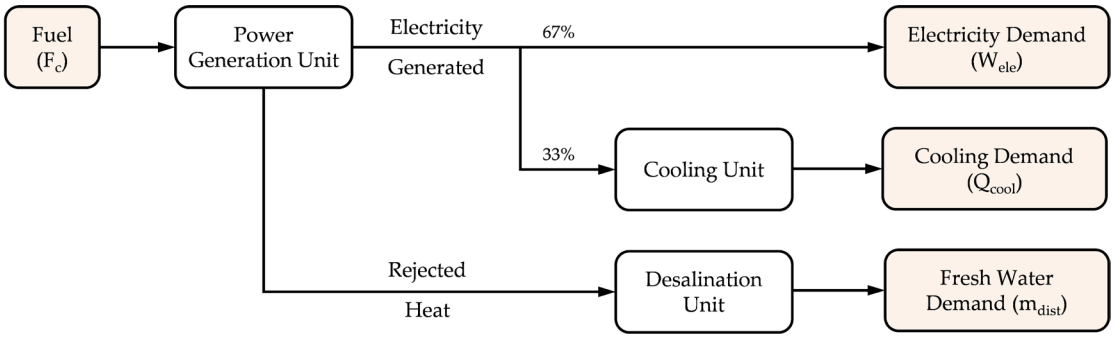

Fig. 3. Energy flows of the proposed CCDP system.

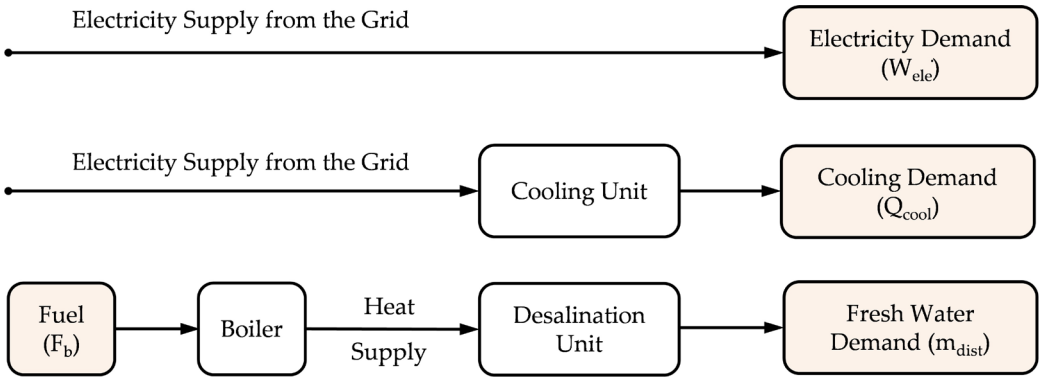

Fig. 4. Energy flows of the reference separate CCDP systems.

Table 1
Main operating condition assumptions for the CCDP system

Parameter	Value	Unit
Rankine cycle		
Temperature (T_3)	200	°C
Boiler saturation temperature	170	°C
Condenser saturation temperature	70	°C
Gas refrigeration cycle		
Low pressure	70	kPa
Pressure ratio	2.5	
Heat exchanger 1 (regenerator) effectiveness	60	%
Temperature (T_{10})	15	°C
MED	35	%
MED number of effects	14	Effects
Top brine (first effect) temperature	66	°C
Temperature rise of seawater in preheater (dT)	2.3	°C
Pressure difference between the effects of MED (dP)	1	kPa
Seawater temperature	27	°C
Seawater salinity	35,000	ppm
Others		
$\dot{m}_{hs}$	1	kg/s
$\dot{Q}_{hs}$ (steam at 200°C) rate of heat source input per unit mass	1,940	kJ/kg
Cooling ratio	33	%
Shaft efficiency	95	%
Turbine isentropic efficiency (η_T)	85	%
Pump isentropic efficiency (η_p)	85	%
Compressor isentropic efficiency (η_C)	80	%
Boiler efficiency (η_b)	85	%
Ambient temperature (T_o)	35	°C
Natural gas price	1.9	$/MMBtu

The Rankine power, gas refrigeration cycles, MED unit, and aforementioned equations are solved simultaneously for steady operating conditions (fluid states and mass, energy, and exergy flows) based on the assumptions shown in Table 1. The thermodynamic properties of water, air, helium, carbon dioxide, etc. are calculated at each point in the system by calling on engineering equation solver routines.

3.3. Model validation

The mathematical model was validated by comparing the RC, ORC, and gas refrigeration cycles individually and independently with the related work in the literature [14,15,25–28]. The obtained results of all individual models were within ±0.5% MED same reference conditions. Table 2 demonstrates the MED single model validation by showing good agreement with the related work in literature [16,29–31] under the same operating conditions of the references.

Table 2
Validation of the MED model

	Current model	Reference	Difference (%)
Freshwater production (kg/h) [16]	2,897	2,992	3.2
Exergy efficiency [32]	6.2	6.0	3.3
Performance ratio [16]	9.25	9.6	3.6

4. Results and discussion

Figs. 5–9 depict the impact of input parameter variations such as the gas refrigeration sub-cycle's pressure ratio, the Rankine sub-cycle's condenser temperature (T_1), the heat exchanger (regenerator) effectiveness (ε_{HX1}), and the MED number of effects. Exergy efficiency (η_{exergy}), electrical power, cooling capacity, freshwater capacity, and PESR are considered to compare the energy consumption and system productivity. PESR is used to compare the proposed CCDP system with the stand-alone reference systems from an energy-savings point of view. Although the results discuss three different refrigerants, namely air, helium, and carbon dioxide, the electrical power output, cooling capacity, and water production are only shown for air because the same pattern is anticipated. It is worth noting that the study is conducted at a fixed thermal energy input rate of 1940 kW_{th}, which corresponds to the value of enthalpy of vaporization of water at 200°C at 1 kg/s mass flow rate.

4.1. Sensitivity to the pressure ratio (r_p)

Fig. 5(a) shows that the exergy efficiency of the CCDP system increases significantly before it levels off as the pressure ratio increases. It can be observed that the exergy efficiency of the combined system only peaks when helium (He) is used as a refrigerant at a pressure ratio of 3.5. Fig. 5(b) demonstrates the effect of pressure ratio on electrical power output, cooling capacity, and water production when air is used as a refrigerant. At a pressure ratio of about 1.5, the gas refrigeration sub-cycle reaches its optimum operating point (maximum COP) as reflected by the cooling capacity in Fig. 5(b) with only a negligible decrease in the electrical power capacity (to the point that cannot be observed in the figure). Consequently, the rise in the rejected heat by the gas refrigeration sub-cycle leads to an increase in the heat absorption by the MED unit, which increases the freshwater production capacity. Because the electrical power output is constant with respect to the pressure ratio, the PESR is directly dependent on the cooling capacity. Fig. 5(c) shows that the PESR of the CCDP system peaks where the gas refrigeration sub-cycle COP peaks for different refrigerants. Unlike a conventional stand-alone cooling cycle, such a combined system is potentially attractive for industrial applications that require freshwater, power, and refrigeration (cryogenics) where very low temperatures are desirable, as shown in Fig. 5(d), without sacrificing the overall system performance and productivity.

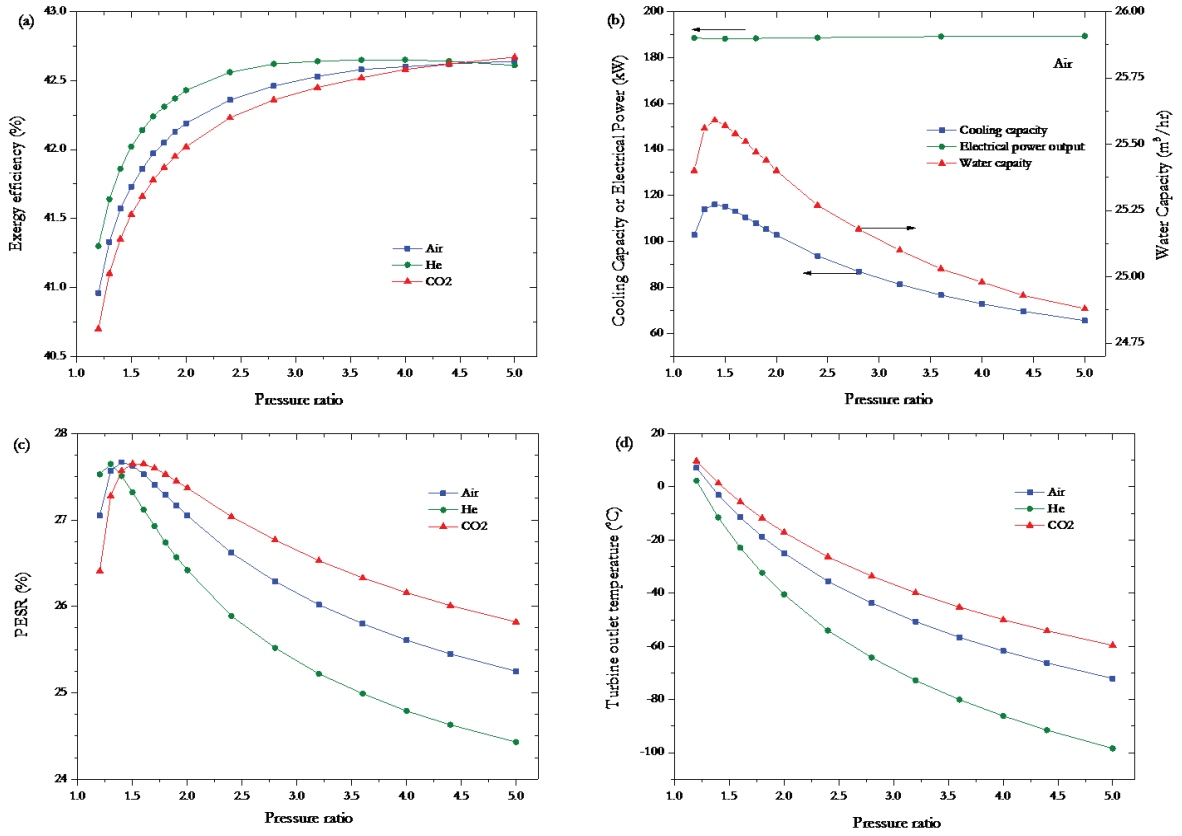

Fig. 5. Effect of the pressure ratio (r_p) of the gas refrigeration sub-cycle on (a) exergy efficiency, (b) electrical power, cooling capacity, and water production, (c) PESR, and (d) gas turbine outlet temperature (T_9) of the proposed CCDP system for different refrigerants (air, He, and CO_2).

4.2. Sensitivity to the Rankine sub-cycle condenser temperature (T_1)

The exergy efficiency of the CCDP system decreases significantly as the condenser temperature (T_1) of the Rankine sub-cycle increases as shown in Fig. 6(a). When air is employed as a refrigerant, the electrical power output increases remarkably as the condenser temperature decreases as depicted in Fig. 6(b). Moreover, since our baseline model assumes that one third of the produced shaft power is used to drive the gas refrigeration cycle, the cooling capacity increases as the electrical power output increases (condenser temperature decreases). Thus, the PESR rises notably as the electrical power output and cooling capacity increases (condenser temperature decreases) as shown in Fig. 6(c). At the same condenser temperature and pressure ratio, the PESR associated with helium is the lowest due to the low output gas turbine temperature. The freshwater production increases marginally with increasing condenser temperature.

4.3. Sensitivity to the reverse Brayton cycle regenerator effectiveness (ε_{HX1})

For the reason that the refrigerant leaves the cooling coil at relatively low temperature and is highly desirable to enter the gas turbine at low temperature, a heat exchanger (regenerator) is vital to recover the cool refrigerant internally. Fig. 7(a) shows that as the regenerator effectiveness increases, the exergy efficiency slightly increases. It can be observed that the exergy efficiencies for different refrigerants are larger at lower regenerator effectiveness, converge as ε_{HX1} increases. As the regenerator effectiveness rises, the electrical power output remains constant, while cooling and freshwater capacities increase slightly as shown in Fig. 7(b). Likewise, the PESR increases with increasing regenerator effectiveness in which the growth differs from only a minor effect when CO_2 is employed to none when He is used as shown in Fig. 7(c). Even though the regenerator effectiveness has a slight effect on cooling capacity regardless of the refrigerant type, the PESR is more sensitive to the water production, which is the case when carbon dioxide is used due to the higher heat rejected which is eventually absorbed by the MED unit.

4.4. Sensitivity to the cooling ratio

Based on the type of application, electrical power and cooling demands fluctuate during the day and time of the year which makes control of any polygeneration system very important. Our proposed CCDP system allows the cooling subsystem (gas refrigeration sub-cycle) to be connected or disconnected easily. Therefore, we define the cooling ratio as the fraction of the electrical power consumed by the gas

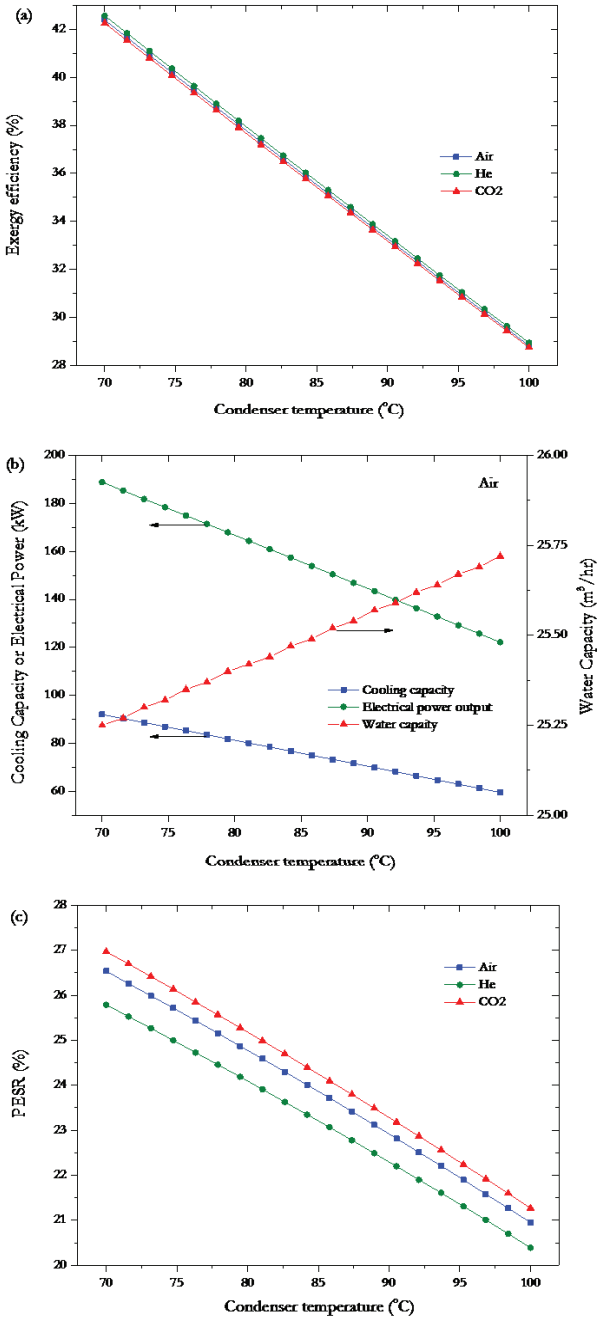

Fig. 6. Effect of the Rankine sub-cycle condenser temperature (T_1) on (a) exergy efficiency, (b) electrical power, cooling capacity, and water production, and (c) *PESR* of the proposed CCDP system for different refrigerants (air, He, and CO_2).

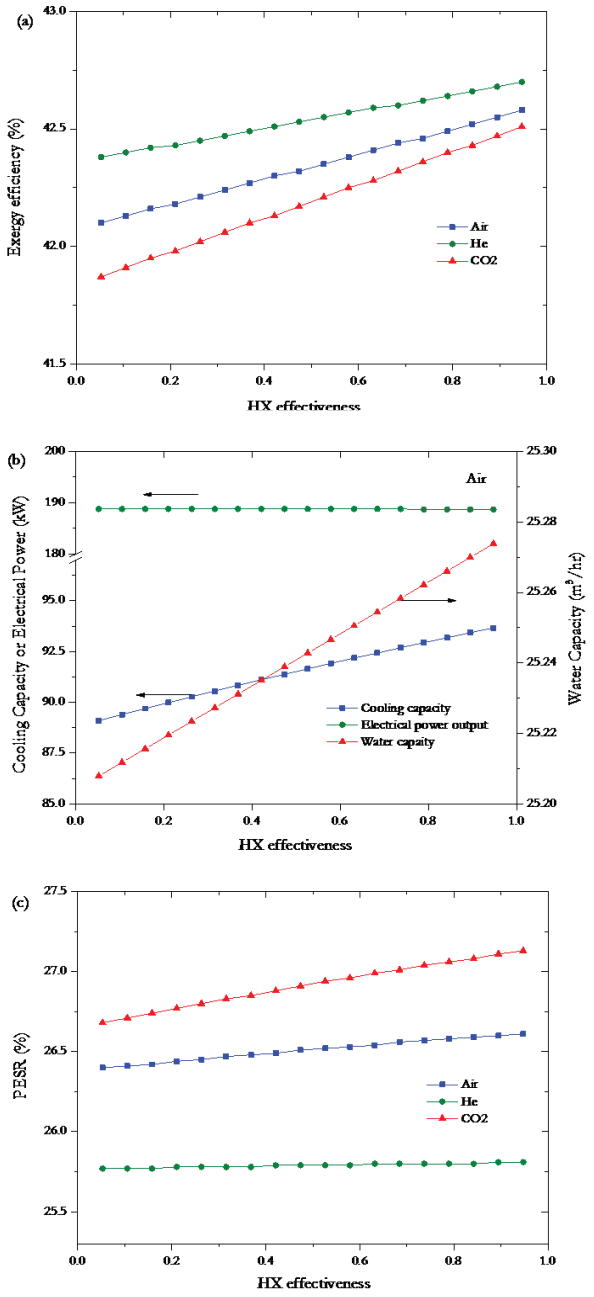

Fig. 7. Effect of the reverse Brayton cycle heat exchanger (regenerator) effectiveness (ε_{HX1}) on (a) exergy efficiency, (b) electrical power, cooling capacity, and water production, and (c) PESR of the proposed CCDP system for different refrigerants (air, He, and CO_2).

refrigeration sub-cycle to the total electrical power produced by the Rankine power sub-cycle. Fig. 8(a) shows that the exergy efficiency decreases steeply from about 55% when zero cooling is generated to about 15% when zero electrical power is generated. When air is employed as a refrigerant, the CCDP system is capable of generating between 290 kW_e of electrical power output and 22 m^3/h of freshwater production at a cooling ratio = 0. On the other hand, the CCDP system can produce about 275 kW_{th} of cooling and 30 m^3/h of freshwater at a cooling ratio = 1, as shown in Fig. 8(b). Furthermore, the PESR decreases as the cooling ratio increases, as shown in Fig. 8(c), at different decreasing (negative) rates of change based on the type of refrigerant. Similar to the last case, the PESR is a strong function of water capacity, which changes as the heat rejected by the gas refrigeration sub-system is absorbed by the MED preheating process.

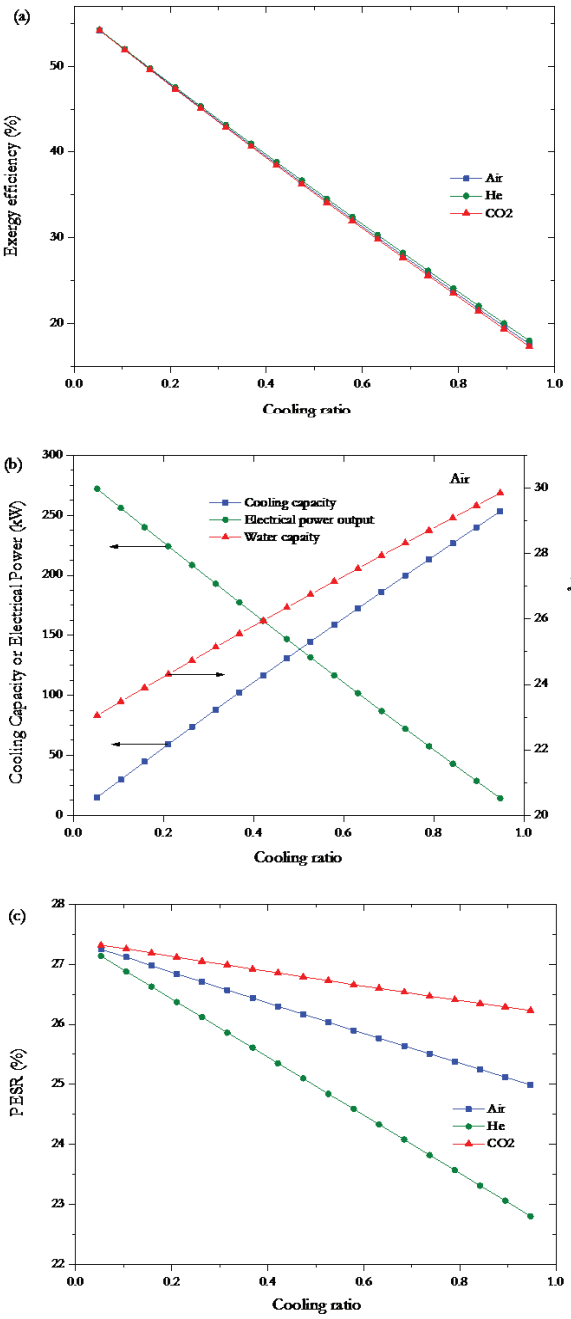

Fig. 8. Effect of the cooling ratio on (a) exergy efficiency, (b) electrical power, cooling capacity, and water production, and (c) PESR of the proposed CCDP system for different refrigerants (air, He, and CO_2).

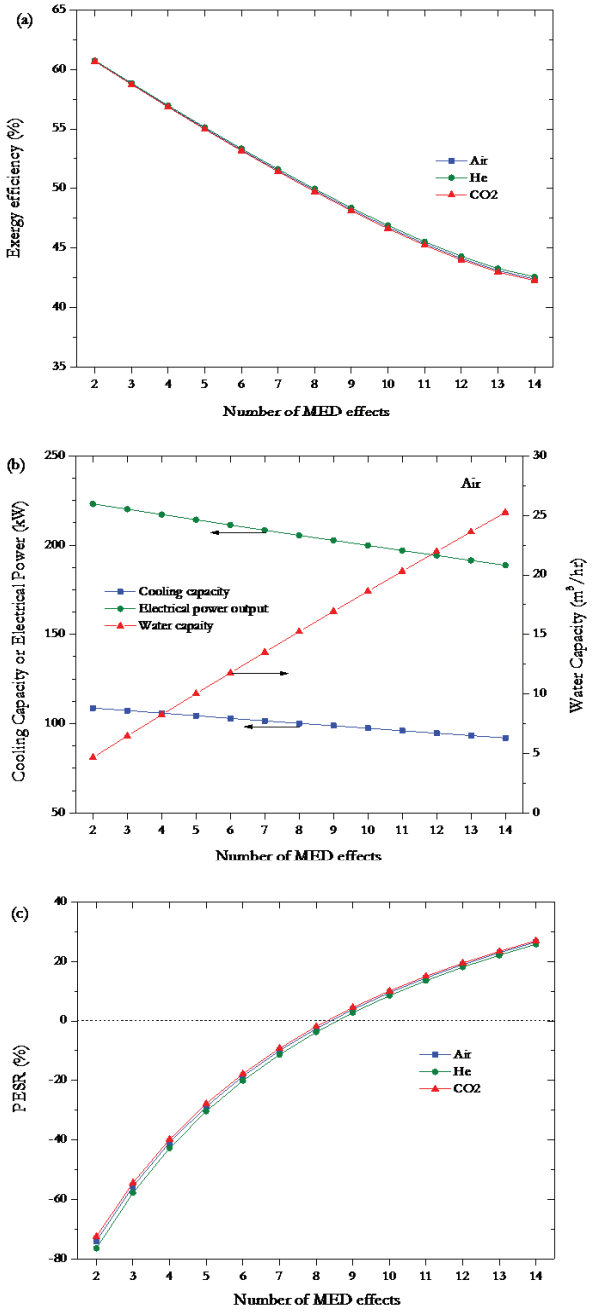

Fig. 9. Effect of the MED number of effects on (a) exergy efficiency, (b) electrical power, cooling capacity, and water production, and (c) PESR of the proposed CCDP system for different refrigerants (air, He, and CO_2).

4.5. Sensitivity to the MED number of effects

Fig. 9(a) depicts that the exergy efficiency sharply decreases as the MED number of effects increases due to the high exergy destruction associated with required pumping system compared with the exergy saved by the MED unit. Nevertheless, the freshwater capacity increases significantly as the MED number of effects increases as shown in Fig. 9(b). Consequently, the PESR increases as the freshwater production increases (MED number of effects increases) as shown in Fig. 9(c). The CCDP system becomes feasible from an energy perspective when the MED number of effects exceeds eight effects (units), which proves that the PESR is a strong function of water production by the MED unit. The reduction of the electrical power output, as the MED number of effects increases, is due to the electrical power consumption associated with the required pumping system, which leads to a reduction in the cooling capacity as well.

4.6. Sensitivity to the Rankine sub-cycle working fluid

Unlike the conventional steam RC, an ORC uses working fluids that are suitable for converting low-temperature heat into electricity [33]. In our case, using an ORC instead of a conventional steam RC is more desirable due to one major advantage: the slope of the saturated vapor curve (right curve of the dome) is almost vertical. Consequently, there is no need for superheating or reheating the vapor before the turbine inlet because the vapor quality problem at the turbine outlet does not exist in the ORC [34]. Under the main assumptions listed in Table 1 (except pressure ratio = 1.4), Table 3 shows a comparison of our proposed CCDP system using different combinations of working fluids and refrigerants for the Rankine sub-cycle and gas refrigeration sub-cycle, respectively. It can be observed from Table 3 that the CCDP system that employs water and air as working fluid and refrigerant, respectively, attains the highest cooling capacity of 116.1 kW_{th} and PESR of 27.7%. Similarly, the CCDP system with water and helium (He) produces the maximum electrical power output of 188.3 kW_e with a maximum exergy efficiency of 41.9%. In the same way, the highest water production of 26.6 m^3/h is achieved by the CCDP system that uses propane as the ORC working fluid due to the low ORC efficiency (highest heat rejection by the condenser).

4.7. Economic impact of the polygeneration system

For the sake of a simple economic analysis, thermal energy is assumed to be supplied to both the combined and stand-alone systems by burning natural gas. The annual fuel savings is calculated as follows and results for different working fluids are shown in the last column of Table 3:

$$\mathrm{AFS} = \frac{C_f \cdot \mathrm{PSRE} \cdot F_s \cdot \mathrm{AOH} \cdot (3600\mathrm{s/hr})}{\mathrm{HHV} \cdot \rho_{\mathrm{fuel}}} \tag{9}$$

where C_f ($/m^3) is the fuel specific cost, AOH is annual operation hours (assuming 24 h per day, and 345 d per year), HHV (kJ/kg) is the higher heating value in, and ρ_{fuel} (kg/m^3) is the fuel density [35]. It can be seen from Table 3 that when water and air are used as working fluids, for instance, the proposed CCDP system can save $502/year per unit kW_{th} heat input compared with stand-alone systems. Alelyani et al. [18] estimated the total annual costs of an MED unit with matching water capacity to be $1.05M/year. Accordingly, our proposed CCDP system is capable of cutting the total annual costs by almost 93% compared with a stand-alone MED unit when water and air are used as a working fluid and refrigerant, respectively.

5. Conclusions

This paper proposes the opportunity of a CCDP system based on the Rankine and gas refrigeration (reverse Brayton) cycles, and MED water desalination unit. The proposed CCDP system harnesses heat rejection by the RC condenser to drive the desalination unit and part of the shaft work to drive the gas refrigeration cycle. At a fixed thermal energy input of 1940 kW_{th} (via steam at 200°C), our thermodynamic

Table 3
Comparison of the proposed CCDP system using different working fluid combinations

Power cycle working fluid	Cooling cycle refrigerant	Power cycle efficiency (%)	Cooling cycle COP	T_9 (°C)	Exergy efficiency (%)	Power capacity (kW_e)	Cooling capacity (kW_{th})	Water capacity (m^3/h)	PESR (%)	Annual fuel savings per unit heat input (($/$kW_{th}$)/year)
Water[a]	Air	17.8	1.25	–3.0	41.6	188.2	116.1	25.6	27.7	502
Water[a]	CO_2	17.8	1.23	1.4	41.4	188.3	114.0	25.6	27.6	500
Water[a]	He	17.8	1.22	–11.6	41.9	188.3	112.8	25.5	27.5	498
R123[a]	Air	14.1	1.25	–3.0	35.3	139.9	86.3	25.8	23.5	426
R123[a]	CO_2	14.1	1.23	1.4	35.1	139.9	84.8	25.8	23.4	424
R123[a]	He	14.1	1.22	–11.6	35.5	140.0	83.9	25.8	23.4	424
Isopentane[a]	Air	12.7	1.25	–3.0	32.0	121.5	75.0	25.9	21.8	395
Isopentane[a]	CO_2	12.7	1.23	1.4	31.9	121.5	73.6	25.9	21.7	393
Isopentane[a]	He	12.7	1.22	–11.6	32.2	121.6	72.8	25.9	21.7	393
R245fa	Air	11.8	1.25	–3.0	30.9	109.6	67.6	26.0	20.6	373
R245fa	CO_2	11.8	1.23	1.4	30.7	109.6	66.4	26.0	20.6	373
R245fa	He	11.8	1.22	–11.6	31.1	109.6	65.7	26.0	20.5	371
Isobutene	Air	11.2	1.25	–3.0	29.6	101.6	62.7	26.0	19.8	359

(*continued*)

Table 3 (*continued*)

Power cycle working fluid	Cooling cycle refrigerant	Power cycle efficiency (%)	Cooling cycle COP	T_9 (°C)	Exergy efficiency (%)	Power capacity (kW_e)	Cooling capacity (kW_{th})	Water capacity (m^3/h)	PESR (%)	Annual fuel savings per unit heat input (($/$kW_{th}$)/year)
Isobutene	CO_2	11.2	1.23	1.4	29.4	101.7	61.6	26.0	19.8	359
Isobutene	He	11.2	1.22	–11.6	29.8	101.7	60.9	26.0	19.7	357
R134a	Air	5.9	1.25	–3.0	16.5	32.6	20.1	26.4	12.2	221
R134a	CO_2	5.9	1.23	1.4	16.4	32.6	19.8	26.4	12.2	221
R134a	He	5.9	1.22	–11.6	16.5	32.6	19.5	26.4	12.2	221
Propane	Air	5.0	1.25	–3.0	13.6	21.1	13.0	26.5	10.8	201
Propane	CO_2	5.0	1.23	1.4	13.6	21.1	12.8	26.5	10.8	201
Propane	He	5.0	1.22	–11.6	13.7	21.1	12.6	26.5	10.8	201

[a]ORC boiler pressure is at critical pressure

model shows that the proposed CCDP system is more feasible from an energy-saving perspective when the MED number of effects is more than eight effects (units) compared with separate systems that provide the same services. When water and air are utilized as a working fluid and refrigerant, respectively, the CCDP system is capable of generating around 188 kW_e of electrical power output, 116 kW_{th} of cooling capacity, and 26 m^3/h freshwater capacity for steam at 200°C and a mass flow rate of 1 kg/s. Additionally, the proposed polygeneration system can achieve an exergy efficiency and PESR of approximately 42% and 28%, respectively. Furthermore, we also explored replacing the conventional steam Rankine sub-cycle with an ORC with the aim of using other working fluids that are suitable for converting low-temperature heat into electricity. The results show that working fluids with the lowest ORC energy efficiency produce slightly more freshwater due to the high heat rejection rate. Additionally, employing helium as a refrigerant instead of air allows the CCDP system to achieve the lowest turbine outlet temperature and highest exergy efficiency.

Symbols

CCDP — Combined cooling, desalination, and power
COP — Coefficient of performance
F — Fuel
MED — Multiple-effect distillation
ORC — Organic Rankine cycle
PESR — Primary energy-saving ratio, %
dP — Pressure difference between the effects of MED, kPa
dT — Temperature rise of seawater in preheater, °C
E — Exergy flow rate, kW
h — Specific enthalpy, kJ/kg
h_{fg} — Enthalpy of vaporization, kJ/kg
$\dot{m}$ — Mass flow rate, kg
P — Pressure, kPa
$\dot{Q}$ — Heat flow rate, kW
s — Specific entropy, kJ/kg K
T — Temperature, °C
W — Power, kW
x — Water salinity, ppm

Greek

η — Efficiency, %

Subscripts

b — Boiler
B — brine stream
c — Combined
C — Cell (effect)
con — Condenser
cool — Cooling
D — Demister
Dist — Distilled
ele — Electrical
eva — Evaporator
ex — External surface of the bundle evaporation tubes
F — Flash

HX	—	Heat exchanger
hs	—	Heat source
i	—	Effect number
L	—	Water saturated liquid
M	—	Mixer
min	—	Minimum
o	—	Dead state
P	—	Preheater
ref	—	Reference
rej	—	Rejected seawater
s	—	Separate
th	—	Thermal
v	—	Water saturated vapor

Acknowledgment

A special thanks to the Saudi Arabian Cultural Mission for supporting S.M.A.'s study in the United States of America.

References

[1] M. Elimelech, W.A. Phillip, The future of seawater desalination: energy, technology, and the environment, Science, 333 (2011) 712–717.
[2] H. Li, N. Russell, V. Sharifi, J. Swithenbank, Techno-economic feasibility of absorption heat pumps using wastewater as the heating source for desalination, Desalination, 281 (2011) 118–127.
[3] N. Ghaffour, J. Bundschuh, H. Mahmoudi, M.F.A. Goosen, Renewable energy-driven desalination technologies: a comprehensive review on challenges and potential applications of integrated systems, Desalination, 356 (2015) 94–114.
[4] J.T. McMullan, Refrigeration and the environment—issues and strategies for the future, Int. J. Refrig., 25 (2002) 89–99.
[5] S. Murugan, B. Horák, Tri and polygeneration systems—a review, Renewable Sustainable Energy Rev., 60 (2016) 1032–1051.
[6] S. Anvari, H. Taghavifar, A. Parvishi, Thermo-economical consideration of regenerative organic Rankine cycle coupling with the absorption chiller systems incorporated in the trigeneration system, Energy Convers. Manage., 148 (2017) 317–329.
[7] B. Ortega-Delgado, P. Palenzuela, D.-C. Alarcón-Padilla, Parametric study of a multi-effect distillation plant with thermal vapor compression for its integration into a Rankine cycle power block, Desalination, 394 (2016) 18–29.
[8] G. Mohan, S. Dahal, U.K. Nutakki, A.R. Martin, H. Kayal, Development of natural gas fired combined cycle plant for tri-generation of power, cooling and clean water using waste heat recovery: techno-economic analysis, Energies, 7 (2014) 6358–6381.
[9] M. Akbari, S.M.S. Mahmoudi, M. Yari, M.A. Rosen, Energy and exergy analyses of a new combined cycle for producing electricity and desalinated water using geothermal energy, Sustainability, 6 (2014) 1796–1820.
[10] U. Sahoo, R. Kumar, P.C. Pant, R. Chaudhury, Scope and sustainability of hybrid solar–biomass power plant with cooling, desalination in polygeneration process in India, Renewable Sustainable Energy Rev., 51 (2015) 304–316.
[11] M. Ameri, M. Jorjani, Performance assessment and multi-objective optimization of an integrated organic Rankine cycle and multi-effect desalination system, Desalination, 392 (2016) 34–45.
[12] M. Salimi, M. Amidpour, Investigating the integration of desalination units into cogeneration systems utilizing R-curve tool, Desalination, 419 (2017) 49–59.
[13] S.M. Alelyani, J.A. Sherbeck, N.W. Fette, Y. Wang, P.E. Phelan, Assessment of a novel heat-driven cycle to produce shaft power and refrigeration, Appl. Energy, 215 (2018) 751–764.
[14] Y.A. Cengel, M.A. Boles, Thermodynamics: an engineering approach, Sea, 1000 (2002) 8862.
[15] J.M. Michael, N.S. Howard, Fundamentals of Engineering Thermodynamics, John Wiley & Sons, Hoboken, NJ, USA, 2011.
[16] A. Hatzikioseyian, R. Vidali, P. Kousi, Modelling and Thermodynamic Analysis of a Multi Effect Distillation (MED) Plant for Seawater Desalination, National Technical University of Athens (NTUA), Greece, 2003.
[17] K.M. Bataineh, Multi-effect desalination plant combined with thermal compressor driven by steam generated by solar energy, Desalination, 385 (2016) 39–52.
[18] S.M. Alelyani, N.W. Fette, E.B. Stechel, P. Doron, P.E. Phelan, Techno-economic analysis of combined ammonia-water absorption refrigeration and desalination, Energy Convers. Manage., 143 (2017) 493–504.
[19] M. Rosen, M. Le, Efficiency Measures for Processes Integrating Combined Heat and Power and District Cooling, in Thermodynamics and the Design, Analysis, and Improvement of Energy Systems, AES Vol. 35, ASME, New York, 1995, pp. 423–434.
[20] S. Kang, H. Li, J. Lei, L. Liu, B. Cai, G. Zhang, A new utilization approach of the waste heat with mid-low temperature in the combined heating and power system integrating heat pump, Appl. Energy, 160 (2015) 185–193.
[21] W. Han, Q. Chen, R. Lin, H. Jin, Assessment of off-design performance of a small-scale combined cooling and power system using an alternative operating strategy for gas turbine, Appl. Energy, 138 (2015) 160–168.
[22] H. Li, S. Kang, L. Lu, L. Liu, X. Zhang, G. Zhang, Optimal design and analysis of a new CHP-HP integrated system, Energy Convers. Manage., 146 (2017) 217–227.
[23] F. Verdier, MENA Regional Water Outlook. Part II Desalination Using Renewable Energy Task 1–Desalination Potential, Fichtner, Stuttgart, Germany, 2011.
[24] A. Al-Karaghouli, L.L. Kazmerski, Energy consumption and water production cost of conventional and renewable-energy-powered desalination processes, Renewable Sustainable Energy Rev., 24 (2013) 343–356.
[25] P. Gandhidasan, A simplified model for air dehumidification with liquid desiccant, Sol. Energy, 76 (2004) 409–416.
[26] P. Gandhidasan, Quick performance prediction of liquid desiccant regeneration in a packed bed, Sol. Energy, 79 (2005) 47–55.
[27] A. Khalil, M. Fatouh, E. Elgendy, Ejector design and theoretical study of R134a ejector refrigeration cycle, Int. J. Refrig., 34 (2011) 1684–1698.
[28] S. Varga, A.C. Oliveira, B. Diaconu, Analysis of a solar-assisted ejector cooling system for air conditioning, Int. J. Low Carbon Technol., 4 (2009) 2–8.
[29] F.N. Alasfour, A.O.B. Amer, The feasibility of integrating ME-TVC+MEE with Azzour South Power Plant: economic evaluation, Desalination, 197 (2006) 33–49.
[30] N. Kahraman, Y.A. Cengel, Exergy analysis of a MSF distillation plant, Energy Convers. Manage., 46 (2005) 2625–2636.
[31] I.J. Esfahani, Y.T. Kang, C. Yoo, A high efficient combined multi-effect evaporation–absorption heat pump and vapor-compression refrigeration part 1: energy and economic modeling and analysis, Energy, 75 (2014) 312–326.
[32] K.H. Mistry, R.K. McGovern, G.P. Thiel, E.K. Summers, S.M. Zubair, J.H. Lienhard, Entropy generation analysis of desalination technologies, Entropy, 13 (2011) 1829–1864.
[33] C. Vetter, H.-J. Wiemer, D. Kuhn, Comparison of sub- and supercritical Organic Rankine Cycles for power generation from low-temperature/low-enthalpy geothermal wells, considering specific net power output and efficiency, Appl. Therm. Eng., 51 (2013) 871–879.
[34] S. Quoilin, M. Van Den Broek, S. Declaye, P. Dewallef, V. Lemort, Techno-economic survey of Organic Rankine Cycle (ORC) systems, Renewable Sustainable Energy Rev., 22 (2013) 168–186.
[35] S.R. Turns, An Introduction to Combustion, McGraw-Hill, New York, 1996.

Appendix A

With reference to Fig. 2, the mass and energy balance equations of the MED unit are derived and listed as follows.

A. The flash

$$\dot{m}_{BC_{i-1}} = \dot{m}_{BF_i} + \dot{m}_{vF_i} \tag{A1}$$

$$\dot{m}_{BC_{i-1}} x_{BC_{i-1}} = \dot{m}_{BF_i} x_{BF_i} + \dot{m}_{vF_i} x_{vF_i} \tag{A2}$$

$$\dot{m}_{BC_{i-1}} h_{BC_{i-1}} = \dot{m}_{BF_i} h_{BF_i} + \dot{m}_{vF_i} h_{vF_i} \tag{A3}$$

where $\dot{m}$ is the mass flow rate, x is the water salinity in the flash, i is the effect number, B is the brine stream, C is the cell (effect), F is the flash, and v is the freshwater saturated vapor.

B. The MED evaporator

$$\dot{m}_{BF_i} = \dot{m}_{BC_i} + \dot{m}_{\mathrm{vex}_i} \tag{A4}$$

$$\dot{m}_{vM_{i-1}} = \dot{m}_{LE_i} + \dot{m}_{vE_i} \tag{A5}$$

$$\dot{m}_{BF_i} x_{BF_i} = \dot{m}_{BC_i} x_{BC_i} \tag{A6}$$

$$\dot{m}_{vM_{i-1}} h_{vM_{i-1}} - \dot{m}_{LE_i} h_{LE_i} - \dot{m}_{vE_i} h_{vE_i} = \dot{m}_{\mathrm{vex}_i} h_{\mathrm{vex}_i} + \dot{m}_{BF_i} h_{BF_i} - \dot{m}_{\mathbf{B}F_i} h_{BF_i} \tag{A7}$$

where ex and E represent the external and internal surfaces of the bundle evaporation tubes, respectively; L the freshwater saturated liquid; M the mixer; and D the demister.

C. The demister

$$\dot{m}_{vex_i} + \dot{m}_{vF_i} = \dot{m}_{vD_i} \tag{A8}$$

$$\dot{m}_{vex_i} h_{vex_i} + \dot{m}_{vF_i} h_{vF_i} = \dot{m}_{vD_i} h_{vD_i} \tag{A9}$$

D. The preheater

$$\dot{m}_{vD_i} = \dot{m}_{vP_i} + \dot{m}_{LP_i} \tag{A10}$$

$$\dot{m}_{swP_i} = \dot{m}_{swP_{i+1}} \tag{A11}$$

$$\dot{m}_{swP_i} h_{swP_i} - \dot{m}_{swP_{i+1}} h_{swP_{i+1}} = \dot{m}_{vD_i} h_{vD_i} - \dot{m}_{vP_i} h_{vP_i} - \dot{m}_{LP_i} h_{LP_i} \tag{A12}$$

where P represents the preheater, and SW the seawater feed.

E. The vapor mixer

$$\dot{m}_{vM_i} = \dot{m}_{vP_i} + \dot{m}_{vE_i} \tag{A13}$$

$$\dot{m}_{vM_i} h_{vM_i} = \dot{m}_{vP_i} h_{vP_i} + \dot{m}_{vE_i} h_{vE_i} \tag{A14}$$

F. The liquid mixer

$$\dot{m}_{\mathrm{Distilled}_i} = \dot{m}_{LE_i} + \dot{m}_{LP_{i-1}} + \dot{m}_{\mathrm{Distilled}_{i-1}} \tag{A15}$$

$$\dot{m}_{\mathrm{Distilled}_i} h_{\mathrm{Distilled}_i} = \dot{m}_{LE_i} h_{LE_i} + \dot{m}_{LP_{i-1}} h_{LP_i} + \dot{m}_{\mathrm{Distilled}_{i-1}} h_{\mathrm{Distilled}_{i-1}} \tag{A16}$$

where "Distilled" represents the distilled water in liquid form.

G. The MED condenser

$$\dot{m}_{vM_n} = \dot{m}_{L\mathrm{Con}} \tag{A17}$$

$$\dot{m}_{sw} = \dot{m}_{sw,\mathrm{rej}} + \dot{m}_{swP_n} \tag{A18}$$

$$\dot{m}_{vM_n} h_{vM_n} - \dot{m}_{L\mathrm{Con}} h_{L\mathrm{Con}} = \dot{m}_{sw,\mathrm{rej}} h_{sw,\mathrm{rej}} + \dot{m}_{swP_n} h_{swP_n} - \dot{m}_{sw} h_{sw} \tag{A19}$$

where LCon represents the condensate water vapor in the condenser, rej the rejected seawater, and n the total number of effects.

H. MED system minimum work

The minimum separation work, or least amount of work to separate salt and water, is given by Eq. (A20) [30,32]:

$$\dot{W}_{\min} = \dot{E}_{\mathrm{Brine}} + \dot{E}_{\mathrm{product}} - \dot{E}_{\mathrm{incoming\ SW}} = \dot{E}_{BC_n} + \dot{E}_{\mathrm{Distilled}_n} + \dot{E}_{L\mathrm{Con}} - \dot{E}_{sw} \tag{A20}$$

where $\dot{E}$ is the exergy rate and can be calculated using Eq. (2).